



A Stochastically Generated Geometrical Finite Element Model for Predicting the Residual Stresses of Thermally Sprayed Coatings Under Different Process Parameters

A. Gademoula¹ · K. S. Al-Athel¹ · S. S. Akhtar¹ · A. F. M. Arif²

Submitted: 7 November 2019 / in revised form: 27 February 2020 / Published online: 11 March 2020
© ASM International 2020

Abstract In this work, a 3D stochastic model coupled with a finite element (FE) code is used to investigate the development of residual stresses in thermally sprayed coatings. The residual stresses of a thermally sprayed yttria-stabilized zirconia (YSZ) coating applied to stainless steel substrates are used for this work. The formation of the coating layers was simulated with a 3D stochastic model, SimCoat. Three YSZ coating models with a similar average thickness, but different layers (one-, two-, and three-layer coatings) were obtained by changing three process parameters: the material feed rate, the gun velocity, and the total number of passes. Two 2D slices of each 3D model were taken and converted into FE models using an in-house Python code. An FE simulation was then used to study the combined effect of these process parameters on the development of residual stresses. The variation of in-plane stresses through the thickness for each model was obtained, and a comparison between the developed stresses was conducted. The developed methodology was effective for understanding the effect of the coating process parameters on the development of residual stresses and can be used to

optimize the coating process parameters to obtain the desired residual stresses.

Keywords coatings · finite element · residual stresses · thermal spray · YSZ

Introduction

Ceramic coatings are widely used as a protective thin layer for metallic components that operate under severe conditions. Ceramic materials such as zirconia, silicon carbide, and silicon nitride are commonly used to provide thermal insulation to hot components to improve thermal efficiency and increase the component's service life. Diesel engines and gas turbine blades are mostly coated by thermal barrier coatings developed by thermal spraying techniques (Ref 1-3).

Thermal spraying is considered an economical and effective way of producing ceramic coatings on metallic substrates. In this process, the coating material, which is fed to the thermal spray system in the form of powder, is heated above its melting point and used as small droplets that are accelerated toward a prepared substrate surface. Upon landing on the substrate surface, the particles strike the surface, flatten, rapidly solidify (Ref 4), and then mechanically and chemically bond to each other as the coating thickness accumulates (Ref 5-7). The rapid cooling of the flattened particles (splats) results in huge contraction of the splats, which in turn leads to structural defects and inter-splat cracks (Ref 8-10). When the spaces between the contracted splats are not filled by subsequent splats, randomly distributed voids of different sizes and shapes are created. Additionally, the imperfect contact between splats and unmolten particles and cracks formed by solidification,

This article is part of a special topical focus in the *Journal of Thermal Spray Technology* on Advanced Residual Stress Analysis in Thermal Spray and Cold Spray Processes. This issue was organized by Dr. Vladimir Luzin, Australian Centre for Neutron Scattering; Dr. Seiji Kuroda, National Institute of Materials Science; Dr. Shuo Yin, Trinity College Dublin; and Dr. Andrew Ang, Swinburne University of Technology.

✉ K. S. Al-Athel
kathel@kfupm.edu.sa

¹ Mechanical Engineering Department, King Fahd University of Petroleum & Minerals, Dhahran 31261, Saudi Arabia

² Department of Mechanical Engineering, McMaster University, Hamilton, ON L8S 4L7, Canada

relaxation of the quenching stresses and thermal stresses contribute to the formation of the porous, defective coating microstructure (Ref 4, 5, 11). Because of such structure, the thermo-physical properties of the coating differ from those of the corresponding bulk material (Ref 4).

To obtain uniform properties for thermally sprayed coatings, the particle temperature, diameter, and impact velocity must be carefully controlled. Thermally sprayed coatings' properties are sensitive to several process parameters, such as gun speed, droplet size, temperature, solidification rate, and substrate material. Studying the effect of these parameters experimentally is costly and time-consuming, and different effects are difficult to distinguish. Therefore, computational models are widely used to optimize the coating process parameters (Ref 12, 13).

The major problem in thermally sprayed ceramic coatings on metallic substrates is the development of residual stresses due to the dynamics of the coating particles involved in the spraying process, and the difference in mechanical and thermo-physical properties between the coating and substrate materials (Ref 14). These stresses are inevitable results of the manufacturing and fabrication process and cannot be avoided (Ref 15). It is important to understand the behavior of the residual stresses because they influence the coating's thermal and mechanical properties, such as adhesion strength, thermal shock resistance, and coating service life (Ref 16). The relationship between the residual stresses and coating longevity has been investigated in the literature; for example, McGrann et al. (Ref 17) studied the influence of the residual stresses on the fatigue life of thermally sprayed coatings and found a direct relation between the residual stresses and fatigue life. Araujo et al. (Ref 18) revealed that residual stresses play an effective role in coating adhesion. The failure of TBCs after exposure to several thermal cycles can be attributed to the residual stresses developed during the coating process, the oxidation of the bond coat, the thermal mismatch between coating and substrate materials, sintering, and creep (Ref 19, 20).

Different types of stresses develop during the spray process given as follows. (1) Quenching stresses occur because of the contraction of the splats restricted by their adherence to the substrate or the preceding coating layers. The splats are always tensile in the deposited layers. (2) Thermal mismatch stresses occur after the deposition is completed and the coating has cooled to room temperature. These stresses are induced by the difference in thermal expansion coefficients between the deposited layer and substrate material. The residual stresses can be either compressive or tensile, depending on the materials and the number of coating layers (Ref 14, 16).

Various experimental techniques have been developed to determine residual stresses. These techniques can be

destructive or nondestructive. Destructive techniques are those that destroy the sample to evaluate the internal stresses. The most widely used destructive techniques are hole drilling and the curvature method. Nondestructive methods include x-ray diffraction, neutron diffraction, and ultrasonic methods (Ref 21). The issue with the mentioned experimental techniques is that they do not predict a detailed stress profile along the thickness of the coating. They only give the average value of the residual stresses. Additionally, many are difficult to apply for thin coatings. Various analytical and computational models have been suggested to simulate the variation of the stresses through the coating thickness (Ref 22). Tsui and Clyne (Ref 23) developed an analytical model to predict the residual stress distributions based on the concept of misfit strain. The model combined the stresses due to splat quenching and thermal contraction between coating and substrate during cooling. Most analytical models have been developed based on the theory of elasticity, with several assumptions considered to derive the solution. Recently, computational models have become more common. One commonly used numerical method for predicting residual stresses is the finite element (FE) method. The birth-kill finite element method has been used to consider both deposition and post-deposition stresses. The birth-kill technique is commonly applied to simulate layer-by-layer growth of the deposition stresses (quenching). Killing (or deactivating) an element is obtained by reducing the values of material properties such as conductivity or stiffness to almost zero. This is done by multiplying these properties by a reduction factor mostly taken as 1×10^{-6} . In birth (reactivation), the element is multiplied by a reduction factor equaling unity (Ref 15, 24).

In this study, three stochastically generated FE models are presented to simulate the residual stresses induced during the spraying of YSZ on stainless steel. Three models were developed by varying three process parameters (gun speed, feed rate, and number of passes) while keeping the same average total thicknesses: one-layer, two-layer, and three-layer coatings of YSZ applied on stainless steel. Two 2D slices of each model were taken and converted into a 2D FE model using an in-house Python code. The developed FE models represent a 2D geometry of the coatings with accurate details of the surface roughness and a clear distinction of the interfaces between the coating layers, and can be imported into any commercial FE code. The coating process is then simulated by depositing the layers individually and solving the conduction/convection heat transfer that takes place during the coating process. The residual stress distribution is then compared between the three cases to understand the mechanism of residual stress development between the coating layers.

SimCoat Stochastic Model

The coating geometries were developed using SimCoat (Ref 25), software developed based on a 3D stochastic model to simulate the formation of thermal spray coatings. It can predict coating thickness, roughness, and porosity. In SimCoat, it was assumed that the values of particle temperature (T), speed (V), diameter (D), splat peripheral detachment, and impact point coordinates have random distributions. Measurements showed that the values of the velocity and the temperature of the particles could be represented by a normal probability distribution termed by (μ, σ^2) with probability density function given by:

$$g(x) = \frac{1}{x\sigma\sqrt{2\pi}} \exp\left(-\frac{1}{2\sigma^2}(\ln x - \mu)^2\right), \quad (\text{Eq 1})$$

where g is the distributed variable, μ is the mean of the population, and σ is the standard deviation of the population. This model assumes that the spherical droplet flattens upon impacting the solid surface and forms cylindrical disks. Because the velocity, temperature, and size of each droplet are given, it is possible to analytically predict the final shape of the splat. Pasandideh-Fard et al. (Ref 26) studied the dynamics of the droplet impact on a solid surface. They used energy conservation equations before and after impact to develop an expression for the maximum spread factor:

$$\xi_{\max} = \frac{D_{\max}}{D_0} = \sqrt{\frac{We + 12}{\frac{We}{\sqrt{Re}} + We\sqrt{3St/(4Pe)}}}, \quad (\text{Eq 2})$$

where We is the Weber number ($We = \rho V_0^2 D_0 / \sigma$), ξ_{\max} is the maximum spread factor, D_{\max} is the maximum splat diameter, D_0 is the droplet diameter before impact, Re is the Reynolds number, and St is the Stefan number.

SimCoat defines the computational domain using a 3D Cartesian grid. The domain is divided into small equal cells to track the position and the shape of the coating surface. The volume fraction, which is the fraction of the cell occupied by the coating material, is used to define the coating structure.

$$f_{i,j,k} = \frac{1}{\Delta x_i \Delta y_j \Delta z_k} \int_{\Delta x_i} \int_{\Delta y_j} \int_{\Delta z_k} f_s dx dy dz, \quad (\text{Eq 3})$$

where $f_{i,j,k} = 1$ when the cell is completely filled with material, $f_{i,j,k} = 0$ when the cell is completely empty or the whole volume of the cell is a pore, and $0 < f_{i,j,k} < 1$ when the cell is partially filled. The coating process parameters are then used as input data to simulate the coating structure. The input data include (Ref 27):

- substrate properties: the length and width of the substrate and the maximum number of grids in the three directions;
- in-flight conditions of the particles and their transportation properties: the mean values of particle diameter, temperature, velocity, dispersion angle, and the standard deviation of each value;
- spray gun conditions: the initial position, standoff distance, and step size; and
- coating material properties.

In this work, SimCoat has been used to simulate the coating process and obtain a 3D geometrical representation of the coating layers. Three process parameters were varied: material feed rate, gun speed, and total number of passes. The substrate size was fixed at $1 \times 1 \text{ mm}^2$, and the coating material was selected to be yttria-stabilized zirconia (YSZ). The computational domain was divided into 1000 cells in the X direction; the program automatically specified the number of cells in the Y direction (1000 cells in this case) from the already assigned substrate dimensions and the number of cells in the X direction.

Table 1 lists the statistical information used in the three models. The particle's diameter, velocity, and temperature are the most important parameters that influence the coating microstructure. The main temperature of the particle was selected to be above the melting point of YSZ, which indicates higher deposition efficiency (Ref 27). The spray dispersion angle can be specified from the diameter covered by the gun and the distance between the substrate and the gun. It was assumed that it has a normal distribution along the axis of the spray gun with a standard deviation of 2.5° . Several models were simulated to select the relevant dispersion angle standard deviation. It was observed that when using a value smaller than 2.5° , the particles are concentrated in certain regions of the substrate, which results in an unrealistic rough coating system. However, when using larger values, the particles will scatter out of the substrate because a relatively small computational domain ($1 \times 1 \text{ mm}^2$) is used. The selected value gave a good particle distribution. Parizi et al. (Ref 27) reported that the standard deviation of the dispersion angle is normally less than 10° . Table 1 lists the spray gun positions, where the gun is moving along the X direction to complete one pass. The gun then steps 0.5 mm in the Y direction to start the next pass. The layer is completed when the whole substrate is covered, and the new layer starts. After covering the whole substrate, the gun will move back half a step size along the Y direction and starts moving in the X direction to build a new layer (Ref 25); following the first pass, the gun will return to use the original step size until the new layer is covered. The initial gun position was chosen as half of the step size (-0.25 mm) to ensure that

Table 1 Coating process parameters

Particle information	Mean value	Standard deviation
Droplet size (diameter in micron)	50	2
Droplet temperature (Celsius)	2550	5
Droplet velocity (m/s)	219	5
Dispersion angle (°)	0	2.5
Spray gun distance from substrate, mm	80	...
Initial gun position in X direction, mm	− 0.25	...
Step size in Y direction, mm	0.5	...

Table 2 Variation between process parameters for the three models

Parameter	Model		
	One-layer	Two-layer	Three-layer
Gun velocity in X direction, m/s	0.25	0.25	0.3
Total no. of passes	3	5	7
Material loading rate, kg/s	0.0009 (54 g/min)	0.0006 (36 g/min)	0.00055 (33 g/min)

passes overlap, to produce good particle distribution, and to avoid peak formation. Because the initial gun position is out of the substrate and the step size is half the width of the substrate, three passes were needed to cover the whole substrate and create the first layer. Only two passes were needed to create each subsequent (second and third) layer because the gun will start from a position parallel to the substrate edge. (Initial gun position is equal to zero.) SimCoat provides the average coating thickness, average roughness, and percentage of pores as simulation results. It should be noted that the roughness represents an arithmetic average of the height of the surface peak from a hypothetical perfectly smooth plane.

One-Layer Model

Table 2 lists the material feed rate, total number of passes, and gun velocity assigned for this model. The combination of these parameters was selected to produce a coating thickness around 200 μm. Because of the gun step size, its initial position, and substrate dimensions, three passes were needed to cover the substrate and create one layer. It was assumed that the gun moves in the X direction at a constant speed. Figure 1(a) shows a 3D plot of the deposition, in which the legend refers to the coating thickness. The results of the run are reported in Table 3.

Two-Layer Model

In this model, two parameters were varied to maintain an average thickness of 200 μm. The material loading rate was reduced, and the total number of passes was increased. Because of the step size and initial gun position, five passes were needed to create two layers. The gun velocity was left constant at 0.25 m/s. The parameters are listed in Table 2. Table 3 shows the results of the simulation. Figure 1(b) shows a 3D view of the YSZ-coated layer.

Three-Layer Model

Because the number of layers is increasing, the spray gun speed should be increased and/or the material feed rate should be decreased to produce thinner layers. The gun speed was increased to 0.3 m/s, and the material feed rate was decreased to 0.00055 kg/s. The final coating structure is shown in Fig. 1(c). The details of the three-layer coating are listed in Tables 2 and 3.

FE Modeling

To simulate the thermal stresses developed by the thermal spraying process, the simulated coating geometry must be converted into an FE model. An in-house code was built to extract the coating roughness and convert it into text format, and another Python code was built to convert the text file into a 2D CAD geometry that can be imported into any

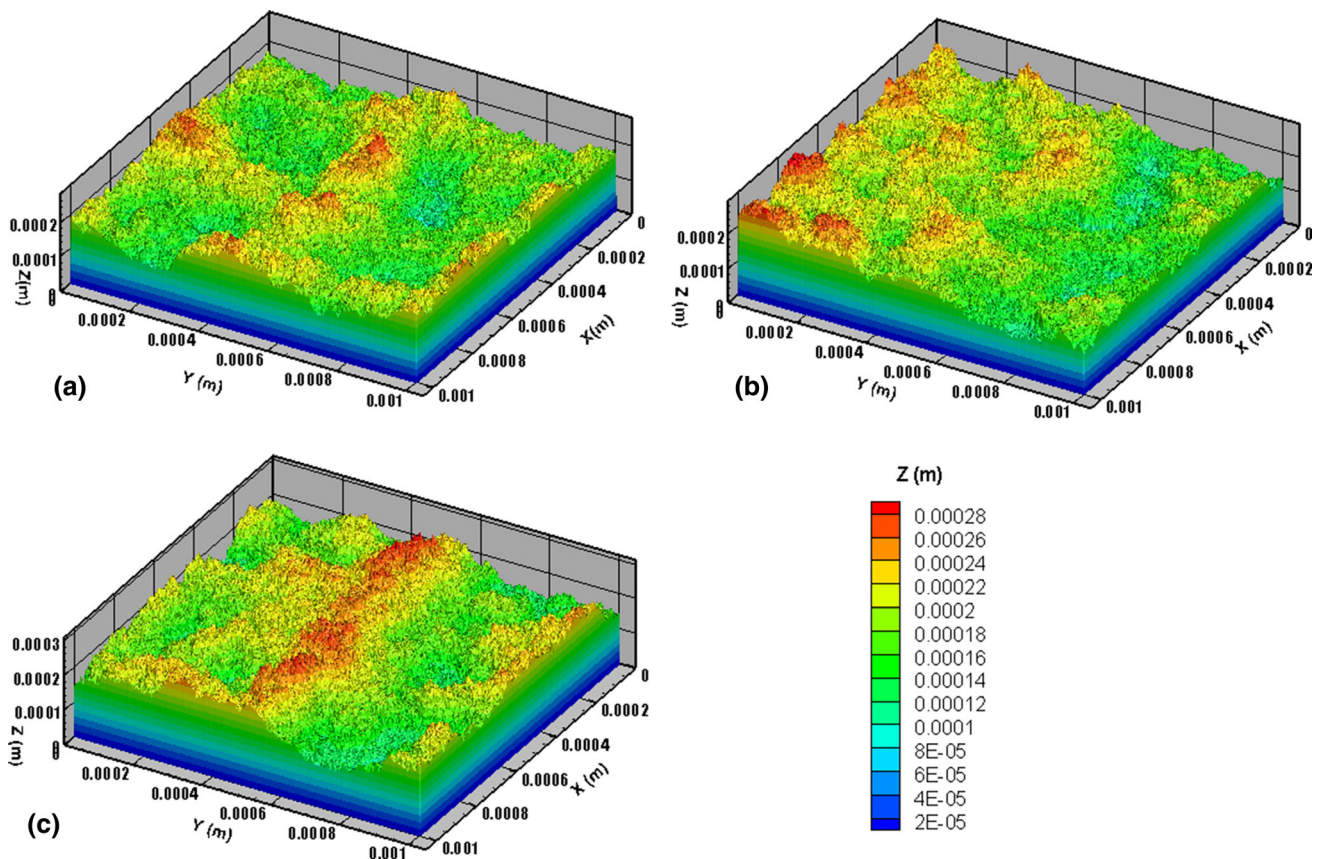


Fig. 1 Isometric view of YSZ coating in (a) one-layer, (b) two-layer, and (c) three-layer models

Table 3 Coating simulation results

Parameter	One-layer model		Two-layer model		Three-layer model	
	X direction	Y direction	X direction	Y direction	X direction	Y direction
Porosity, %	1.01	1.076	1.0391	1.21629	0.9779	0.934
Thickness, μm	171	200	171	191	188	247
Roughness, μm	28	13	25	17	29	12

commercial FE software. SimCoat was linked with TECPLOT software to provide data visualization (Fig. 1). TECPLOT provides the data of the 3D simulation of the coating structure in terms of several planes, each plane divided into small cells. The coordinates and porosity values of each cell were stored in a data spreadsheet. Each model includes 100 planes (indexed from 1 to 100) parallel to the XZ plane.

Two slices (planes) were selected, indexed as 5 and 30 of each model parallel to the X-axis. Only the roughness values were extracted, while geometrical porosity was neglected by assuming that the coating surface was completely solid. Adding pores would affect studies investigating crack propagation, which could be an extension of this work. As for predicting the deposition residual stresses between the coating layers, it is reasonable to assume that

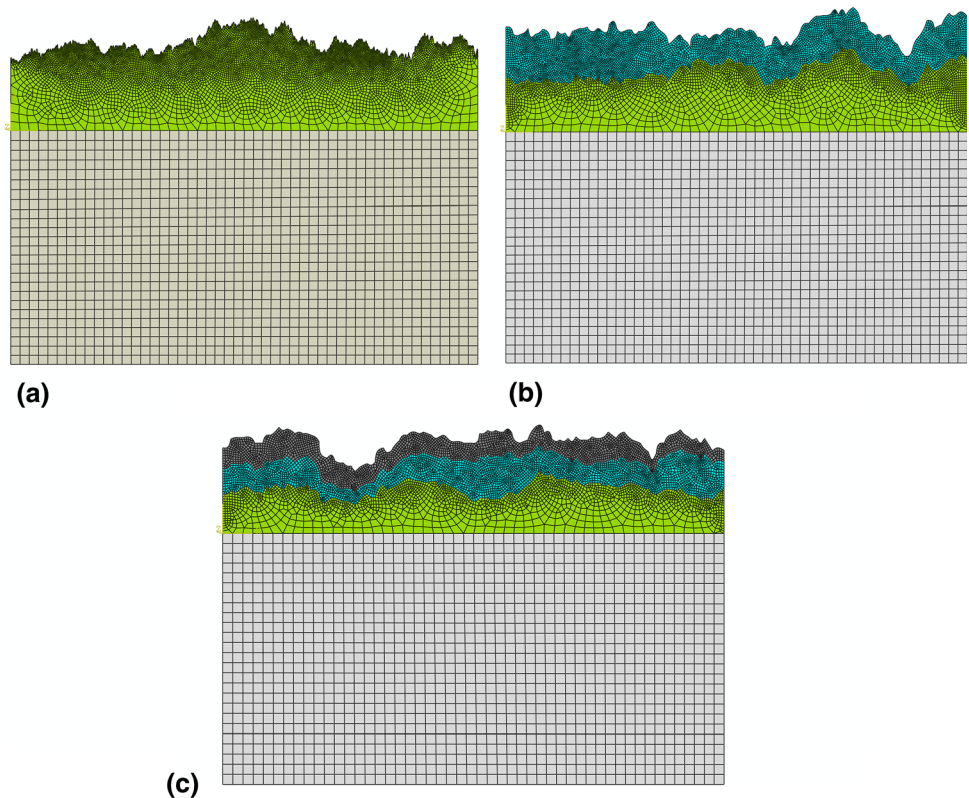
the effect of geometrical pores is neglected. However, it is important to note that the material properties are those of the material with the pores presented within them. Two-dimensional FE models are considered because they represent the worst case in terms of strength. The average thickness was calculated for each model (listed in Table 4), and all models had very close thickness values. The substrate thickness is 0.5 mm. Plane 5 of the one-, two-, and three-layer models is shown in Fig. 2.

ABAQUS (Ref 28) was used as the finite element solution tool to conduct the stress analysis. In the one-layer model, the coating is adhered to the substrate with tie constraints at the interface. In the two- and three-layer models, tie constraints are applied between the substrate and the bottom layer and between subsequent layers. Periodic boundary conditions are applied at the edges.

Table 4 Average thickness and number of elements of the selected slices

Model	Plane	Average thickness micron	Thickness STD, micron	Total no. of elements	Type of element	
					CPS4RT	CPS3T
One-layer model	Plane 5	190	19	11,343	10,839	504
	Plane 30	188	22	11,050	10,516	534
Two-layer model	Plane 5	219	22	9527	9302	225
	Plane 30	220	23	9955	9713	242
Three-layer model	Plane 5	189	25	9283	9029	254
	Plane 30	189	21	8945	8606	339

Fig. 2 Meshing of slice no. 30 in (a) one-layer, (b) two-layer, and (c) three-layer models



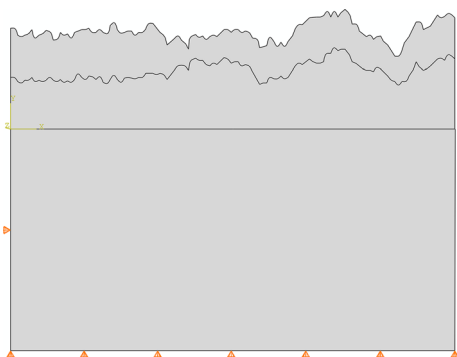
Material properties of stainless steel and YSZ were assigned to the substrate and coating, respectively, as listed in Table 5. To consider stress relaxation due to plastic deformation, plastic properties were defined for both coating and substrate. The initial temperatures for substrate and coating were set to 700 and 2550 °C, respectively. Coupled temperature–displacement transient analysis with multiple time steps was conducted. During spraying, heat transfers from the molten particles by two mechanisms. The first is conduction to the substrate or the previously deposited layer due to the higher initial temperature of the molten-sprayed particles. During solidification, the latent heat associated with the phase change from liquid to solid will be released and conducted to the underlying layers and

substrate. The second mechanism is the heat loss at the bottom surface of the substrate and the top surface of the coating because of natural convection cooling. In the two-layer and three-layer models, layer-by-layer buildup was assumed. Model change interaction was applied to deactivate and reactivate elements to simulate the deposition of the two and three coating layers using the birth-kill FE technique.

In the two-layer model, the top layer was deactivated (killed) in the first step and reactivated in the second step. At the third time step, natural convection was applied to cool the assembly to room temperature. In the three-layer model, the middle and top layers were activated in the second and third steps, respectively. In the fourth time step,

Table 5 Material properties of YSZ and stainless steel (Ref 29)

Property	YSZ	301 stainless steel
Density (kg/m ³)	5890 @ liquid and solid state	7900
Latent heat (J/kg)	7.07E+05	...
Specific heat (J/kg K)	713 @ liquid state 580 @ solid state	477
Thermal conductivity, (W/m K)	2.32 @ liquid state 2.0 @ solid state	14.1
Coefficient of thermal expansion (1/ °C)	9.68E−6 @ 20 °C 10.34E−6 @ 1000 °C 11E−6 @ 2527 °C	16.6E−6 @ 100 °C 17.6E−6 @ 300 °C 18.6E−6 @ 500 °C 19.5E−6 @ 700 °C
Elastic modulus <i>E</i> (GPa)/Poisson ratio	63.4/0.21 @ 20 °C 28.33/0.21 @ 2000 °C 26.67/0.21 @ 2522 °C 3E−3/0.4 @ 2532 °C 3E−3/0.4 @ 3000 °C	200/0.3 @ 700 °C 0.2/0.4 @ 1400 °C
Melting point (°C)	2527 °C	
Heat transfer coefficient of air (W/m ² K)	20	20
Yield strength (MPa)	30 (tensile) 300 (compressive)	Johnson–Cook parameters: <i>A</i> = 310, <i>B</i> = 1000, <i>C</i> = 0.07, <i>n</i> = 0.65, <i>m</i> = 1

**Fig. 3** Applied boundary conditions and path created for residual stress variation along the thickness

the coated substrate was cooled. To conduct the analysis, the models were discretized into small elements, as shown in Fig. 2, with a more refined mesh at the rough surfaces to capture the geometrical details of the roughness. The number of elements and types of element for each model are listed in Table 4. Plane stress analysis was conducted for each case.

Results and Discussion

The thermal stresses developed because of the thermal mismatch between the substrate and coating materials during and after deposition for one-, two-, and three-layer

models are investigated in the longitudinal direction. For each case, a path starting from 0.3 mm substrate depth up to the top surface of the coating was created. It was located exactly in the middle of the substrate length to exclude the effect of the free boundaries (Fig. 3).

Figure 4, 5, and 6 shows the stress distribution contours for the three models before and after cooling, while Fig. 7, 8, and 9 shows the residual stresses before and after cooling for the middle path shown in Fig. 3. Figure 4(a) shows the quenching stress distribution, while Fig. 4(b) shows the residual stresses due to the thermal mismatch at the end of the cooling step of the one-layer model. These stresses are graphically shown in Fig. 7. The stresses developed in YSZ coating because of quenching are tensile with a maximum value around 108 MPa, while those generated in the coating because of thermal mismatch are mostly compressive with a maximum of 135 MPa. In the thermal stress profile, the stress is also higher at the coating–substrate interface and decreases to close to zero at the free surfaces. It has been reported that the maximum stress is always at the interface (Ref 30, 31) and that the residual stresses developed inside the coating particles upon its deposition and rapid solidification are always tensile. Adhesion to the substrate or previously deposited splats restricts particle contraction and induces tensile stresses (Ref 4). The low magnitude of the quenching stress is attributed to the plastic material properties, which are considered to have a stress relaxation effect due to interfacial sliding and

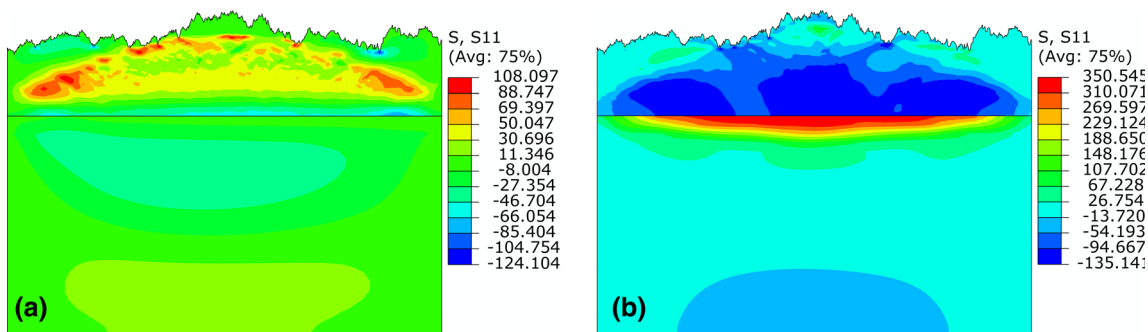


Fig. 4 Residual stresses in the one-layer model: (a) quenching and (b) final thermal stresses

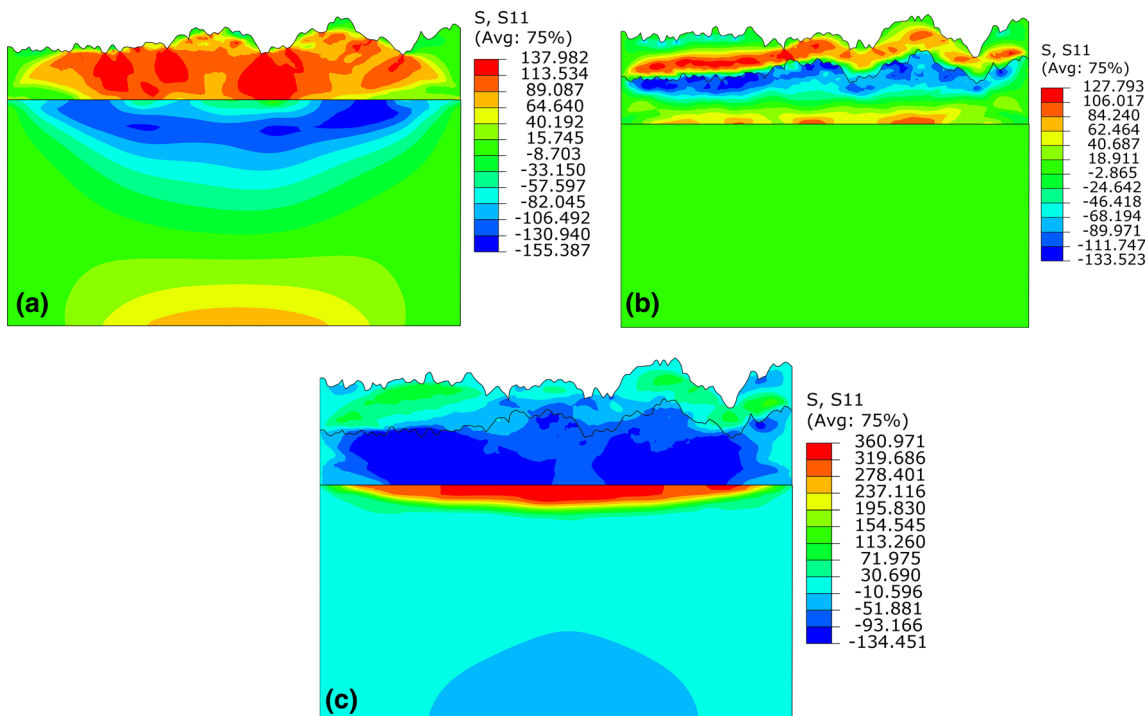


Fig. 5 Residual stresses in the two-layer model: (a) quenching of the bottom layer, (b) quenching of the top layer, and (c) final thermal stresses

microcracking associated with the ceramic coating (Ref 4, 32). The residual stresses developed in the two-layer model during the deposition and cooling are shown in Fig. 5 and 8. The stresses developed after the deposition of the bottom and the top layers are shown in part (a). As with the one-layer model, the deposition of the bottom layer induces tensile stresses. However, the stress values show a significant increase in quenching stresses. Stokes and Looney (Ref 33) analytically studied the dependence of the quenching stress on deposited thickness and found that increasing the deposited coating layer’s thickness reduces tensile quenching stresses. This effect can be clearly observed by comparing Fig. 5(a) and (b). Moving to the deposition of the top layer, there is a clear significant change in the deposit stress profile. The stress at the upper part of the bottom layer has changed from tensile to

compressive, while the compressive stresses in the substrate decreased to zero. This can be explained in that continuing the deposition of material on the top of the previously deposited layer will develop compressive stress under the current deposited one. The contraction of the new particles will be impeded by the old underlying solidified splats. The stress-free state produced in the substrate can be attributed to the balance between the tensile and compressive stresses that occurred within the coating layers. Figure 6 and 9 shows the stress contours and profile for the three-layer model. Similarly, the stresses are higher at the interface between the substrate and coating, where spallation usually occurs. The maximum stresses developed at the interface are 350 and – 134 MPa on the substrate and coating sides, respectively. The residual stress change in the coating/substrate may result in cohesion loss and

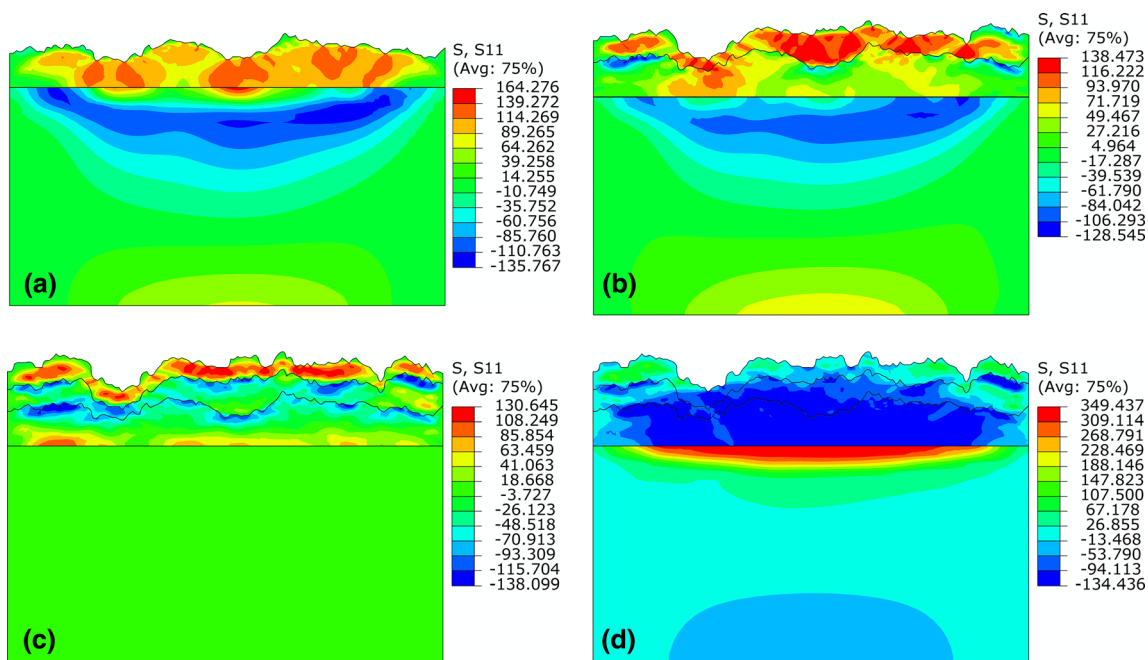


Fig. 6 Residual stresses in the three-layer model: (a) quenching of the bottom layer, (b) quenching of the middle layer, (c) quenching of the top layer, and (d) final thermal stresses

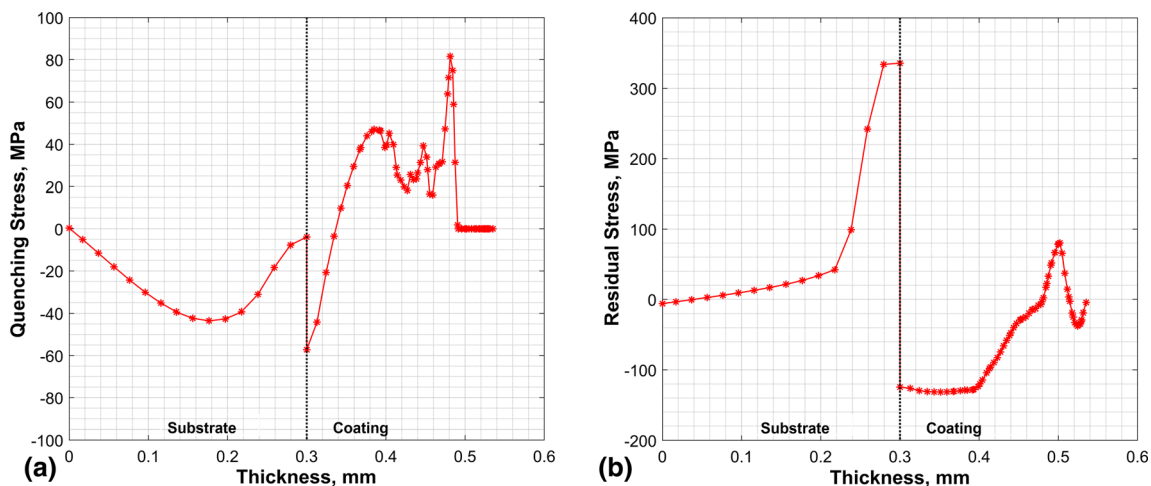


Fig. 7 Residual stresses in the one-layer model: (a) quenching and (b) final residual stresses

consequently reduce the coating longevity. Figure 6(a), (b), and (c) shows the distribution of stresses developed during the deposit of three YSZ layers on the stainless steel substrate. In this case, the gun is moving fast, thus producing thin layers. The increase in quenching stresses within the coating layers confirm what was written previously about the stresses' dependence on coating thickness; the quenching stresses are highest (around 130 MPa) on the coating side. Usually, microcracking associated with ceramic materials is believed to reduce the quenching stresses to lower values compared with metals (Ref 32). The resultant residual stresses in the three-layer model are

shown in Fig. 6(d). There is no difference in the final residual stresses developed in the three coating models. This can be explained because the mismatch of the thermal expansion coefficients of the different materials is the dominant source of the residual stresses here. In most regions on the coating side, the final stresses are around -135 MPa. Thermal mismatch stresses are compressive in ceramic coatings because they possess a low thermal expansion coefficient compared with the underlying substrate. Although the final residual stresses are almost the same in the three coating models, they have different maximum stress locations that would affect the crack

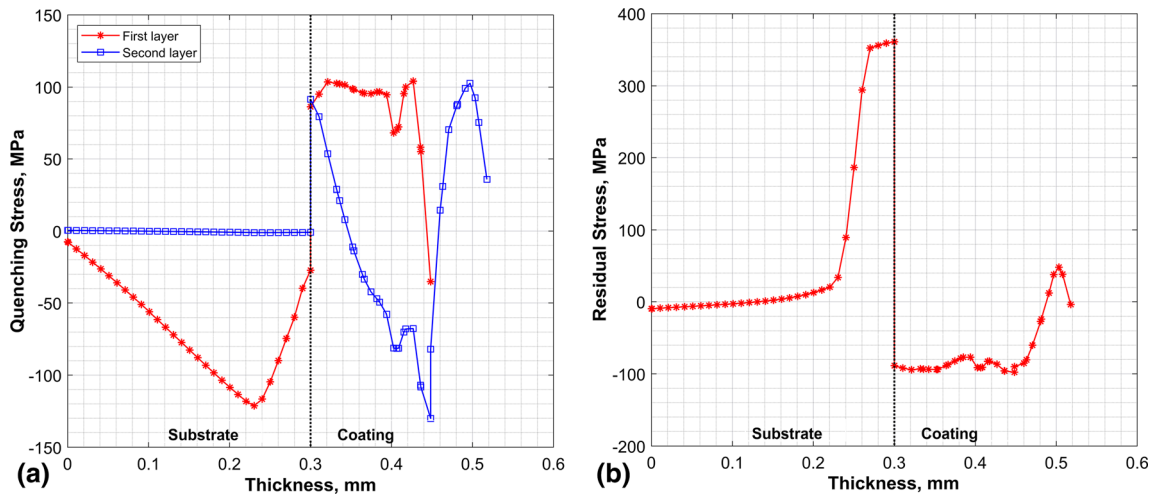


Fig. 8 Residual stresses in the two-layer model: (a) quenching and (b) final residual stresses

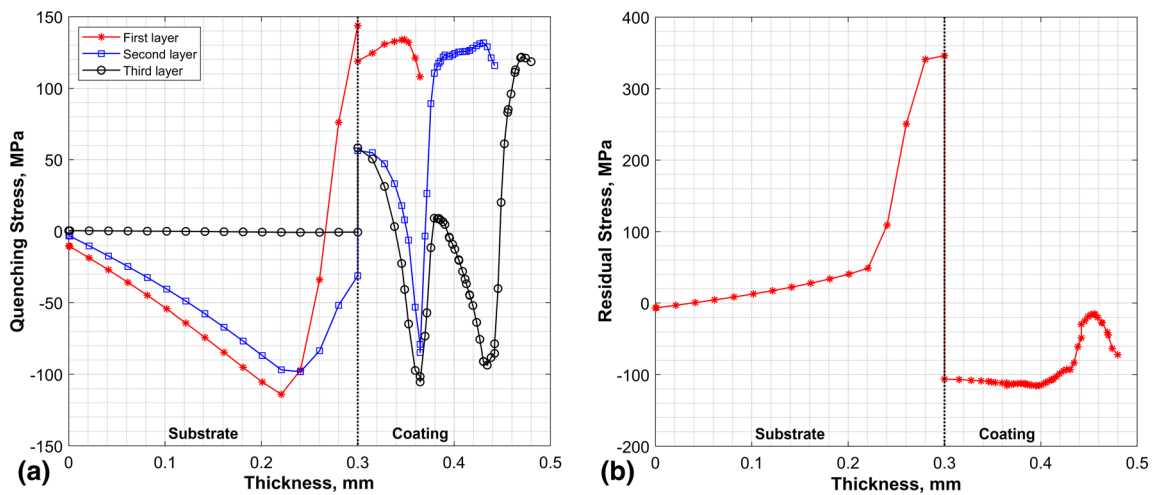


Fig. 9 Residual stresses in the three-layer model: (a) quenching and (b) final residual stresses

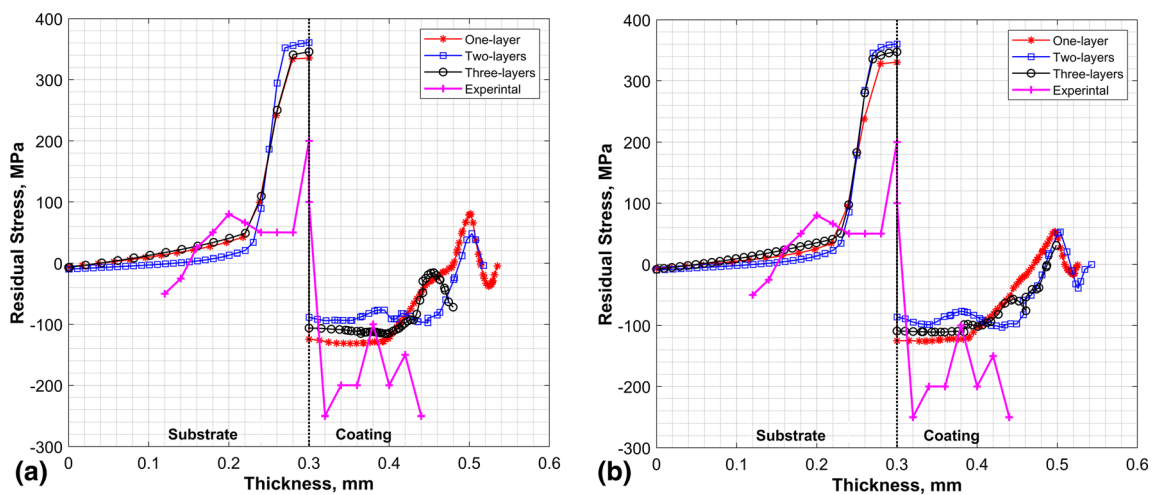


Fig. 10 Thermal residual stresses in the one-layer, two-layer, and three-layer models and experimental values for (a) slice 30 and (b) slice 5

propagation, and hence, the microstructural details due to their different process parameters. The results show that depositing a certain coating thickness using different sets of process parameters leads to different quenching stress distributions. The same study was conducted for the second slice (slice No. 5); the combined results for each slice are shown in Fig. 10(a) and (b). The results show no major difference between the curves in each figure, which indicates an independence of the results in terms of the plane selection and that the 2D slice selection provides general results for the whole coating. Abubaker et al. (Ref 24) experimentally studied the internal stress induced in YSZ coating applied to stainless steel. They used the incremental hole drilling method to determine the residual stresses. Their coating sample was deposited in six passes with a final coating thickness of 150 microns. Stresses acting in YSZ coating are plotted in Fig. 10. Stress profiles obtained in our work are in close agreement with those measured experimentally. It is important to note the difference in process parameters and hence the differences in values. However, the change between the tensile and compressive states and the behavior of the residual stresses was the same.

Conclusion

This work presented a detailed numerical model to investigate the combined influence of varying the coating process parameters on the variation of residual stresses for coatings with different numbers of layers.

The residual stresses predicted using the models were obtained for the quenching stage and the thermal mismatch during the cooling stage. The results generally showed that the process parameters have no significant effect on the thermal mismatch results, and the thermal mismatch is mainly dominated by the material properties, that is, the coefficient of thermal expansion, coating, and substrate. Notably, even though the properties are temperature dependent, the difference in the values of one material at different temperatures is much less than the difference between the materials. However, the results showed a clear difference in the stresses during the deposition process. The model predicted the quenching stresses as it showed a clear stress increase as the number of layers increased. Differences of 19 and 9 MPa in the tensile and compressive stresses, respectively, were observed between the one- and the two-layer models and of 22 and 12 MPa between the one- and three-layer models. Even for the thermal stresses, the differences between the three models are located in the high stresses. This shows that optimizing the process parameters to have fewer layers for a desired thickness is much more desirable in terms of the developed quenching

stresses and would ultimately minimize the number of microcracks that developed during deposition. This can be used in future work to simulate the crack initiation during the quenching stage. The process parameters were examined in terms of the number of layers produced to achieve the same average coating thickness, but a separate study can also be performed on the individual process parameters.

Acknowledgments The authors would like to acknowledge the support of King Fahd University of Petroleum & Minerals (KFUPM) through DSR Project # FT161016.

References

1. S. Gong and Q. Wu, Chapter 6. Processing, Microstructures and Properties of Thermal Barrier Coatings by Electron Beam Physical Vapor Deposition (EB-PVD), *Thermal Barrier Coatings*, 2011, p 115-131.
2. A.M. Noor, F.N. Sharuddin, and U.M. Basheer, Ceramic Materials for Coating Application in Turbocharged Automotive Engine: A Review, AAT2016, Istanbul, October, 2016
3. V. Teixeira, Numerical Analysis of the Influence of Coating Porosity and Substrate Elastic Properties on the Residual Stresses in High Temperature Graded Coatings, *Surf. Coat. Technol.*, 2001, **146-147**, p 79-84
4. L. Chen, Chapter 7. Processing, Microstructures and Properties of Thermal Barrier Coatings (TBCs) by Plasma Spraying (PS), *Thermal Barrier Coatings*, 2011, p 132-160.
5. L. Chen and G. Yang, Epitaxial Growth and Cracking Mechanisms of Thermally Sprayed Ceramic Splats, *J. Therm. Spray Technol.*, 2018, **27**, p 255-268
6. L. Chen and G. Yang, Epitaxial Growth and Cracking of Highly Tough 7YSZ Splats by Thermal Spray Technology, *J. Therm. Spray Technol.*, 2018, **7**, p 17-29
7. L. Chen and G. Yang, Hetero-Orientation Epitaxial Growth of TiO₂ Splats on Polycrystalline TiO₂ Substrate, *J. Therm. Spray Technol.*, 2018, **27**, p 880-897
8. J. Matejcek, R. Musalek, and J. Veverka, Materials and Processing Factors Influencing Stress Evolution and Mechanical Properties of Plasma Sprayed Coatings, *Surf. Coat. Technol.*, 2019, **371**, p 3-13
9. L. Chen, G. Yang, C. Li, and C. Li, Edge Effect on Crack Patterns in Thermally Sprayed Ceramic Splats, *J. Therm. Spray Technol.*, 2017, **26**, p 302-314
10. L. Chen, G. Yang, C. Li, and C. Li, Hierarchical Formation of Intrasplat Cracks in Thermal Spray Ceramic Coatings, *J. Therm. Spray Technol.*, 2016, **25**, p 959-970
11. L. Chen, L. Gao, and G. Yang, Imaging Slit Pores Under Delaminated Splats by White Light Interference, *J. Therm. Spray Technol.*, 2018, **27**, p 319-355
12. R. Ghafouri, J. Mostaghimi, S. Chandra, and M. Charmchi, A Stochastic Model to Simulate the Formation of a Thermal Spray Coating, *J. Therm. Spray Technol.*, 2003, **12**, p 53-69
13. A. Fardan and R. Ahmed, Modeling the Evolution of Residual Stresses in Thermally Sprayed YSZ Coating on Stainless Steel Substrate, *J. Therm. Spray Technol.*, 2019, **28**, p 717-736
14. C. Lyphout, P. Nysten, A. Manescu, and T. Pirling, Residual Stresses Distribution through Thick HVOF Sprayed Inconel 718 Coatings, *J. Therm. Spray Technol.*, 2008, **17**, p 915-923
15. A.A. Abubakar, A.F.M. Arif, K.S. Athel, and S.S. Akhtar, Modeling Residual Stress Development in Thermal Spray

- Coatings: Current Status and Way Forward, *J. Therm. Spray Technol.*, 2017, **26**, p 1115-1145
16. S. Kuroda and T.W. Clyne, The Quenching Stress in Thermally Sprayed Coatings, *Thin Solid Films*, 1991, **200**, p 49-66
 17. R.T.R. McGrann, D.J. Greving, J.R. Shadley, E.F. Rybicki, T.L. Kruecke, and B.E. Bodger, The Effect of Coating Residual Stress on the Fatigue Life of Thermal Spray-Coated Steel and Aluminum, *Surf. Coat. Technol.*, 1998, **109**, p 59-64
 18. P. Araujo, D. Chicot, M. Staia, and J. Lesage, Residual Stresses and Adhesion of Thermal Spray Coatings, *Surf. Eng.*, 2013, **21**, p 35-40
 19. M.R. Far, J. Absi, G. Mariaux, and S. Shahidi, Modeling of the Residual Stresses and their Effects on the TBC System After Thermal Cycling Using Finite Element Method, *Ceram. Mater.*, 2010, **62**, p 275-279
 20. G. Li, L. Wang, G. Yang, C. Li, and C. Li, Combined Effect of Internal and External Factors on Sintering Kinetics of Plasma-Sprayed Thermal Barrier Coatings, *J. Eur. Ceram. Soc.*, 2019, **39**, p 1860-1868
 21. O.S. Zaroog, C.Y.W. Ken, and A.N.A. Manap, Current and Challenge of Residual Stress Measurement Techniques, *Int. J. Sci. Res.*, 2014, **3**, p 210-216
 22. R. Ghafouri-Azar, J. Mostaghimi, and S. Chandra, Modeling Development of Residual Stresses in Thermal Spray Coatings, *Comput. Mater. Sci.*, 2006, **35**, p 13-26
 23. Y.C. Tsui and T.W. Clyne, An Analytical Model for Predicting Residual Stresses in Progressively Deposited Coatings Part I: Planar geometry, *Thin Solid Films*, 1997, **306**, p 23-33
 24. A.A. Abubakar, A.F.M. Arif, S.S. Akhtar, and J. Mostaghimi, Splats Formation, Interaction and Residual Stress Evolution in Thermal Spray Coating Using a Hybrid Computational Model, *J. Therm. Spray Technol.*, 2019, **28**, p 359-377
 25. SIMCOAT, SIMULENT inc. <http://simulent.com/usermanual>
 26. M. Pasandideh-Fard, Y.M. Qiao, S. Chandra, and J. Mostaghimi, Capillary Effects during Droplet Impact on a Solid Surface, *Phys. Fluids*, 1996, **8**, p 650-659
 27. H.B. Parizi, J. Mostaghimi, L. Pershin, and H.S. Jazi, Analysis of the Microstructure of Thermal Spray Coatings: A Modeling Approach, *J. Therm. Spray Technol.*, 2010, **19**, p 736-744
 28. SIMULIA, Abaqus/Standard, 2018
 29. A.A. Abubakar and A.F.M. Arif, A hybrid Computational Approach for Modeling Thermal Spray Deposition, *Surf. Coat. Technol.*, 2019, **362**, p 311-327
 30. Y.Y. Santana, J.G. La Barbera-sosa, M.H. Staia, J. Lesage, E.S. Puchi-cabrera, D. Chicot, and E. Bemporad, Measurement of Residual Stress in Thermal Spray Coatings by the Incremental Hole Drilling Method, *Surf. Coat. Technol.*, 2006, **201**, p 2092-2098
 31. K. Wang, F. Zangzhou, and R.K. Bordia, FEM Modeling of In-Plane Stress Distribution in Thick Brittle Coatings/Films on Ductile Substrates Subjected to Tensile Stress to Determine Interfacial Strength, *Materials*, 2018, **11**, p 1-16
 32. S. Kuroda, T. Fukushima, and S. Kitahara, Significance of Quenching Stress in the Cohesion and Adhesion of Thermally Sprayed Coatings, *J. Therm. Spray Technol.*, 1992, **1**, p 325-332
 33. J. Stokes and L. Looney, Residual Stress in HVOF Thermally Sprayed Thick Deposits, *Surf. Coat. Technol.*, 2004, **177-178**, p 18-23

Publisher's Note Springer Nature remains neutral with regard to jurisdictional claims in published maps and institutional affiliations.